Monte Carlo Simulations of an Experimental Method for Measuring Charge-Changing Cross Sections

R. Prajapat *, Anagha P K, M. Bajzek, J. Eder, E. Haettner, N. Hubbard, C. Hornung, R. Kanungo, S. K. Singh, I. Mukha, S. Purushothaman, C. Scheidenberger, I. Tanihata

Posted Date: 7 April 2026

doi: 10.20944/preprints202604.0374.v1

Keywords: charge-changing cross-section; GEANT4 simulations; carbon isotopes; fragment separator (FRS)

 doi:10.20944/preprints202604.0374.v1

Article

Monte Carlo Simulations of an Experimental Method for Measuring Charge-Changing Cross Sections

R. Prajapat [1,2,*], Anagha P K [1,3], M. Bajzek [1], J. Eder [1], E. Haettner [1], N. Hubbard[1], C. Hornung [1], R. Kanungo [2,4], S. K. Singh [1,5], I. Mukha [1], S. Purushothaman [1], C. Scheidenberger [1,5,6] and I. Tanihata [7,8]

[1] GSI Helmholtz Centre for Heavy Ion Research, Planckstraße 1, 64291 Darmstadt, Germany
[2] Astronomy and Physics Department, Saint Mary's University, Halifax, Nova Scotia B3H 3C3, Canada
[3] Dept. of Physics, University of Calicut, Calicut University P.O Kerala, 673635, India
[4] TRIUMF, Vancouver, British Columbia, V6T2A3, Canada
[5] II. Physikalisches Institut, Justus-Liebig-Universität Gießen, Heinrich-Buff-Ring 16, 35392 Gießen, Germany
[6] Helmholtz Research Academy Hesse for FAIR (HFHF), GSI Helmholtz Centre for Heavy Ion Research, Campus Giessen, 35392 Giessen, Germany
[7] RCNP, Osaka University, Ibaraki, Osaka 567-0047, Japan
[8] School of Physics, Beihang University, Beijing, 100191, China
* Correspondence: r.kumarprajapat@gsi.de

Abstract

Measurements of charge-changing cross-sections were developed as a method for determining proton radii, particularly for unstable, short-lived nuclei. Such cross-sections must be measured with high precision to determine the precise charge radii. However, there are complexities in the experimental method and leading to uncertainties in determining precise nuclear radii. Therefore, good models describing the complex physics of charged-particle interactions are needed in order to validate the experimental method and to estimate the contribution of systematic uncertainties. GEANT4 is a Monte Carlo simulation code that can describe elementary-particles and heavy-ion interactions in a broad range from typical atomic to cosmic-ray energies. An experiment has been performed to measure charge-changing cross-section of carbon isotopes, namely ^{10,11,12}C nuclei, on different secondary reaction targets using the fragment separator FRS at GSI, Darmstadt. This work presents a comparison between the measured spectra of that experiment and the corresponding GEANT4 simulations.

Keywords: charge-changing cross-section; GEANT4 simulations; carbon isotopes; fragment separator (FRS)

1. Introduction

The measurement of charge-changing (σ_{CC}) and interaction (σ_I) cross-sections of radioactive ion beams provides a powerful tool to investigate nuclear structure, particularly of unstable nuclei far from the valley of stability. These observables are directly connected to the proton (R_p) and matter (R_m) radii distributions of nuclei and therefore allow for detailed insight into the spatial structure of exotic systems [1,2]. Over the past decades, advances in radioactive beam production have enabled access to nuclei with extreme neutron-to-proton ratio and short lifetimes, revealing phenomena such as neutron halos and neutron skins [3]. The extraction of reliable nuclear structure information from σ_{CC} and σ_I, however, critically depends on achieving high experimental precision.

In particular, the determination of R_p and R_m at a meaningful level requires cross-section measurements with uncertainties at or below the 1% level. At such a precision, a detailed understanding of systematic effects, detector response, and reaction dynamics becomes essential. Monte Carlo simulations, therefore, play a crucial role, not as a substitute for measurements, but as a tool to validate the experimental method and quantify systematic uncertainties.

 doi:10.20944/preprints202604.0374.v1

At high energies (>1.5 GeV/u), theoretical descriptions of reaction cross-sections are relatively successful [4]. However, at intermediate energies, σ_{CC} and σ_I exhibit a pronounced energy dependence, and the related model predictions begin to diverge. This further emphasizes the importance of precise experimental data to benchmark against theoretical models. Such benchmarking is also important for resolving possible contradictory results. For example, the proposed proton halo structure of ^{8}B, inferred from electromagnetic observables [5], is not consistently supported by interaction cross-section measurements analyzed within Glauber-type approaches [6]. These discrepancies highlight the need for improved precision and careful validation of both experimental techniques and theoretical tools.

The measurements of σ_{CC} were performed within the BARB (Biomedical Applications of Radioactive ion Beams) initiative at GSI, launched to explore the use of positron-emitting carbon and oxygen isotopes for heavy-ion therapy[7–10]. While BARB is motivated by developments in heavy-ion therapy, this contribution focuses on the validation of the experimental method for the precise determination of nuclear reaction cross-sections.

The structure of the paper is as follows: the experimental method are described in Section 2, GEANT4 simulations are provided in Section 3, results are discussed in Section 4, and Section 5 concludes the work.

2. Experimental Method

The experiment was performed using the in-flight fragment separator and magnetic spectrometer FRS [11] at GSI, Darmstadt, Germany. The primary beam of ^{12}C, with an intensity of up to 10^9 ions per spill, was delivered to FRS coupled with the UNILAC [12] and SIS18 [13]. The beam was extracted with a spill length of 2 s.

Secondary beams of interest, ^{10}C and ^{11}C, were produced via nuclear fragmentation of a 470–480 MeV/u primary beam ^{12}C impinged on a 8.0 g/cm^2 beryllium production target located in the target area, F0. The FRS was operated in its standard achromatic mode. Secondary reaction targets and detectors were installed at the focal planes F2 and F4, as shown in Figure 1.

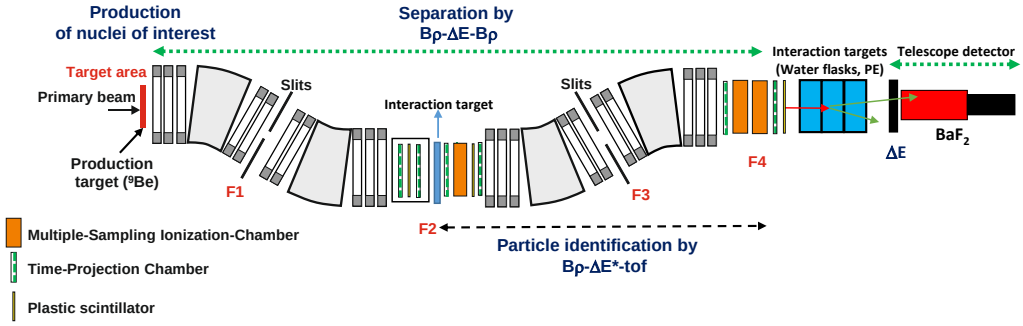

Figure 1. Schematic picture of the FRS main branch with its four stages and focal planes: the target area, F1, F2, F3, and F4. Legend of the used detectors is on bottom left.

The charge-changing cross-section σ_{CC} was measured using the transmission technique as described in Ref. [1]. In this method, the number of incident nuclei before the reaction target ($N_1^{T_{in/out}}$), and the number of outgoing nuclei ($N_2^{T_{in/out}}$) with the same Z or higher ($N_{Z\geq 6}$), were identified and counted for target-in (T_{in}) and target-out (T_{out}) conditions. The σ_{CC} was then deduced using the following equation [Equation 1]:

$$\sigma_{CC} = \frac{1}{n_d} ln\left(\frac{R_{in}}{R_{out}}\right), \tag{1}$$

where $R_{in} = N_2^{T_{in}}/N_1^{T_{in}}$ and $R_{out} = N_2^{T_{out}}/N_1^{T_{out}}$ are the transmission ratios with and without reaction target, respectively, and n_d is the number of target nuclei per cm^2.

 doi:10.20944/preprints202604.0374.v1

For measurements with a reaction target at F2, the isotope of interest was spatially separated using magnetic rigidity ($B\rho$) selection only. Figure 2 shows the calculated position spectrum obtained with the LISE++ [14] simulation tool, illustrating the spatial separation of different carbon fragments at the F2 focal plane. Slits at F2 were set to ±20 mm to select a narrow $B\rho$ range and thereby prevent the other carbon isotopes to hit the F2 reaction target. Charge identification (Z) in front of the F2 reaction target was achieved by measuring the energy deposition of the incoming particles in a plastic scintillator installed upstream of the F2 reaction target.

Downstream of the F2 reaction target, outgoing particles were identified by their charge using the multiple-sampling ionization chamber (MUSIC) and a plastic scintillator detector. The $B\rho$ from F2 to F4 was set to transmit the unreacted beam, allowing for measurement of total interaction cross-section, σ_I. In this case, the incident particles were counted in the same way as for σ_{CC}, while outgoing unreacted nuclei with the same charge and mass were identified and counted using the particle identification information from F2 to F4 focal planes. However, the σ_I were not compared with GEANT4 simulations and therefore not considered further in this work.

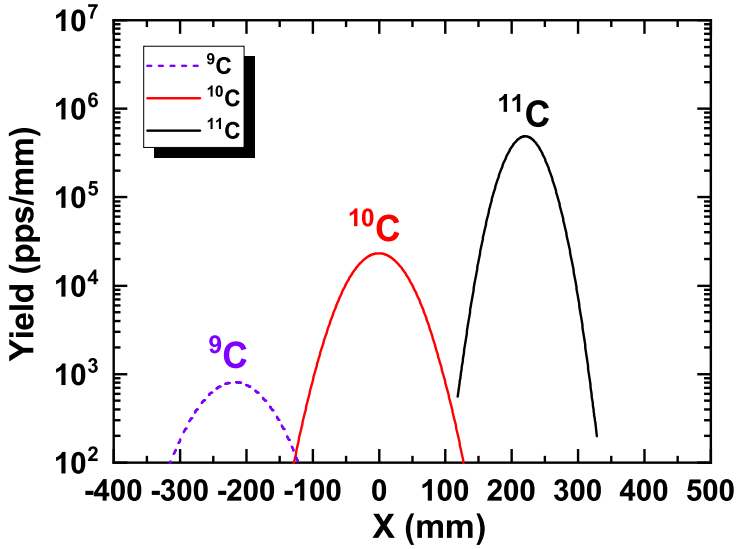

Figure 2. Spatial separation of carbon fragments simulated using the LISE++ [14] with 470 MeV/u of ^{12}C primary beam and ^{10}C as a centered fragment before the secondary reaction target at F2.

At F4, a second set of σ_{CC} measurements was performed simultaneously. For these measurements, the event-by-event identification of incoming ions upstream of the F4 reaction target was achieved using the information of $B\rho$-energy deposition (ΔE)-time of flight (TOF) method. Time projection chambers (TPCs) [15] for tracking, plastic scintillators (SCIs) for TOF [16], and MUSIC for atomic number [17] and measurement were installed as shown in Figure 1. Based on these observables, the mass-over-charge ratio (A/Q) and atomic number of the particles in front of the final focal plane F4 were determined [10].

The outgoing particles downstream of the F4 reaction target were identified using a ($\Delta E - E$) telescope detector consisting of a 10 mm thick plastic scintillator for energy loss (ΔE) measurements and a Barium fluoride (BaF_2) crystal for residual energy (E) measurement.

3. GEANT4 Simulation of the Experiment

Comprehensive GEANT4 Monte Carlo simulations [18,19] were performed to accurately reproduce the experimental beamline configuration. The beam at the TPC focal plane (F2) before the target was defined by transverse positions and angles, expressed as mean ± standard deviation; x = -2.276 ± 9.496 mm, y = 2.92 ± 2.372, θ_x = -1.836 ± 6.756 mrad and θ_y = 1.545 ± 6.778 mrad. These values were derived from experimental measurements. A pure beam was assumed in the simulations. The first simulation reproduced the experimental measurement at the F2 focal plane region of the FRS. The

 doi:10.20944/preprints202604.0374.v1

geometry and positioning of the detectors TPC, the MUSIC, and the SCI were implemented according to the experimental configuration, with the TPC having active dimensions of 24 cm × 6 cm × 7 cm; the MUSIC detector having a box size of 44 cm × 24 cm × 40 cm and an active volume of 22 cm × 10 cm × 30 cm, positioned 12 cm from the TPC surface; and the SCI detector located downstream with dimensions of 22 cm × 10 cm × 0.49 cm at a distance of approximately 12.5 cm from the aluminium window of the MUSIC detector. The simulated interaction region shown in Figure 3 corresponds to the F2 experimental setup presented in Figure 1. The detector response was modeled using standard performance parameters. For the TPC, the intrinsic position resolution was included [15], and similarly for MUSIC and SCI, standard energy-resolution effects were applied to ensure that fragment identification and cross-section measurements reflect the experimental conditions as good as possible.

In the F4 simulation, the geometry consists of a reaction target, a scintillator, and a BaF_2 crystal telescope, as illustrated in Figure 4, which replicates the experimental setup at the F4 focal plane (see Figure 1). The beam profile parameters are taken from experimental measurements, expressed as mean ± standard deviation; x = 0.02403 mm ± 6.388 mm, y = -7.529 ±, θ_x = 3.018 ± 3.809 mrad and θ_y = -4.264 ± = 3.887 mrad. The hexagonal plastic scintillator located 30 cm downstream of the target, modeled using $EJ212$ material that provides fast timing performance. The detector geometry was defined as a 10 cm diagonal hexagonal prism with 1 cm thickness along the beam direction. Optical photon production was implemented with a yield of 10000 photons/MeV and a decay constant of 1.5 ns. The emission spectrum was modeled in the 380-480 nm range, with wavelength-dependent refractive indices included for accurate light transport.

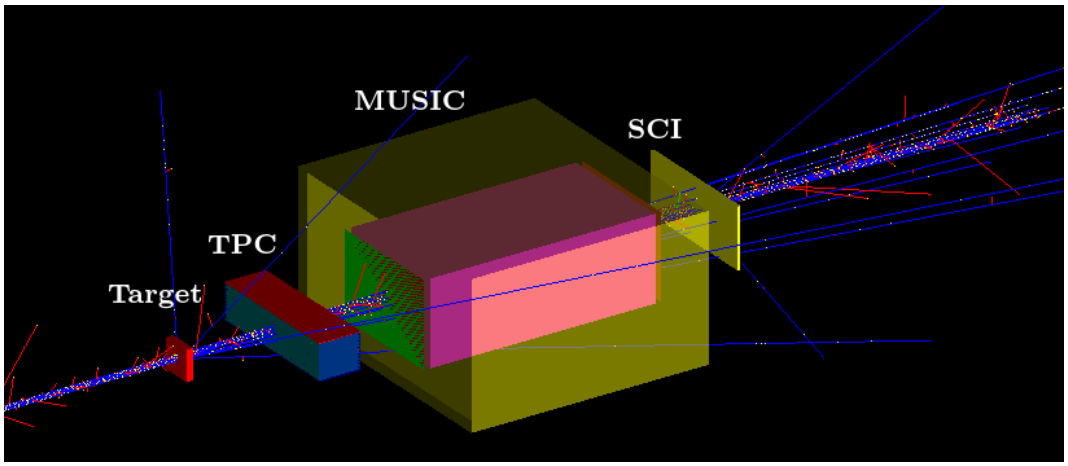

Figure 3. Simulated experimental setup showing incident particle interactions where red and blue trajectories corresponds to negatively and positively charged particles respectively as they transverse the target and beam line detectors TPC, MUSIC, and SCI at F2 focal plane.

Calorimetric measurements were performed using a BaF_2 crystal telescope, a hexagonal prism with a 8.75 cm long diagonal and 14 cm length, which is place at distance of 20 cm from the SCI. The BaF_2 scintillation response was implemented with both fast (0.6 ns, 220 nm) and slow (630 ns, 310 nm) emission components, enabling pulse-shape discrimination. Wavelength-dependent absorption lengths and refractive indices were included to account for self-absorption and optical transport effects. It was used to measure the residual kinetic energy of fragments emerging from the target. Energy loss in both detectors was dominated by electromagnetic ionization processes. Charged particle stopping power was calculated using the GEANT4 electromagnetic framework based on the Bethe–Bloch formalism [19]. Deposited energy was accumulated event-by-event and converted into scintillation light through the *G4Scintillation* process [18].

 doi:10.20944/preprints202604.0374.v1

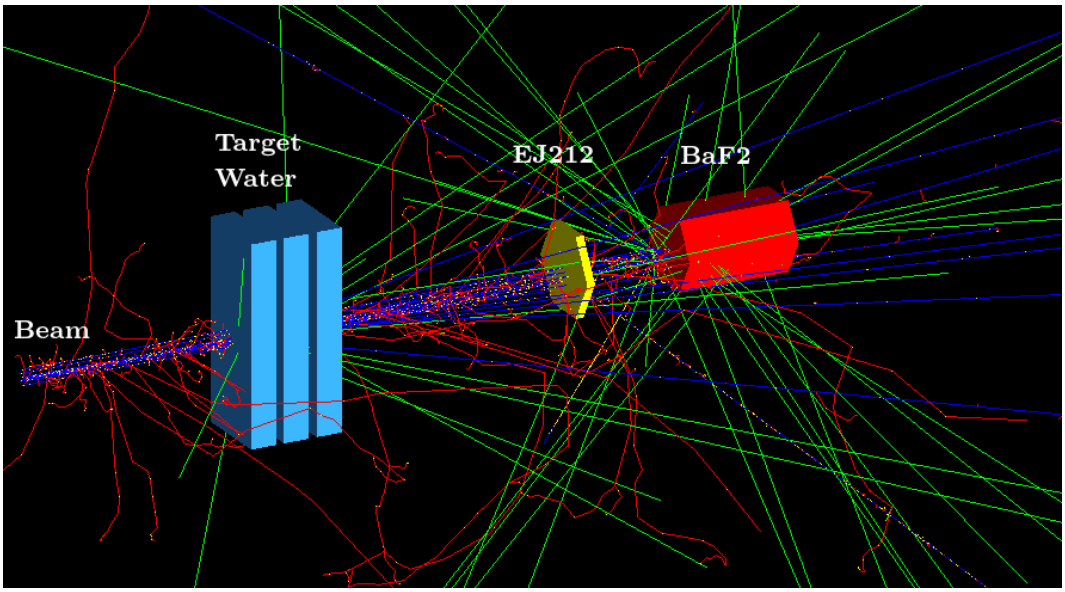

Figure 4. Simulated experimental setup showing particle interactions through water reaction target at F4 focal plane, with red, green, and blue trajectories representing negatively, neutrally, and positively charged particles, respectively, with $EJ212$ and BaF_2 detectors positioned about 30 cm and 50 cm from the target surface.

All simulations were performed using the QBBC_ABLA physics list [20], based on established cascade, string, and de-excitation models [21–23], which provides a consistent treatment of electromagnetic interactions, hadronic reactions, and nuclear fragmentation processes relevant for σ_{CC} studies [24]. Projectile–target collisions were modeled using the hadronic interaction models included in QBBC, followed by statistical de-excitation of excited nuclear remnants. In particular, the ABLA de-excitation model was employed to describe evaporation and fragmentation decay channels of highly excited residual nuclei [25]. This cascade–de-excitation approach is essential for the realistic reproduction of secondary fragment yields and charge-state distributions, which directly influence the extracted charge-changing cross-sections.

Simulation data were stored using GEANT4 ntuple output through the *EventAction* and *SteppingAction* classes. For each event, energy deposition, interaction coordinates, particle identity, and track history (*TrackID*, *ParentID*) were recorded in all volumes. Step-level information was preserved, with separate output collections for the target, scintillator, and BaF_2 systems.

4. Results and Discussion

Figures 5 and 6 show the comparison between the experimentally obtained results with GEANT4 simulations as described below:

4.1. Comparison of the Experimental Data with GEANT4 Simulations

Figure 5(a,b) show the correlation plots between measured energy loss in the MUSIC detector and in the downstream plastic scintillator for a ^{10}C beam with and without a carbon reaction target, respectively, at the F2 focal plane. Similarly, the corresponding GEANT4 simulations are shown in Figures 5(c,d). In experiments and simulations, a pronounced contour ($\Delta E_{MUSIC} \approx 1900$ channels, $\Delta E_{SCI} \approx 2100$ channels) corresponds to the unreacted projectiles. As the energy loss at relativistic energies scales approximately as $\Delta E \propto Z^2$, nuclei with different charges populate distinct blobs in the 2-D spectrum.

When the reaction target is inserted, additional diagonal bands appear below the carbon locus. These are mainly projectile fragmentation products with reduced atomic number, mainly boron (Z=5) and beryllium (Z=4) are visible. The MUSIC detector was not sensitive below Z=5 in this experiment. Whereas, we can notice the other fragmentation products below Z=4 in simulations. This diagonal band is very weak in the target out case, which could be due to possible beam interactions with air gaps and detector material.

 doi:10.20944/preprints202604.0374.v1

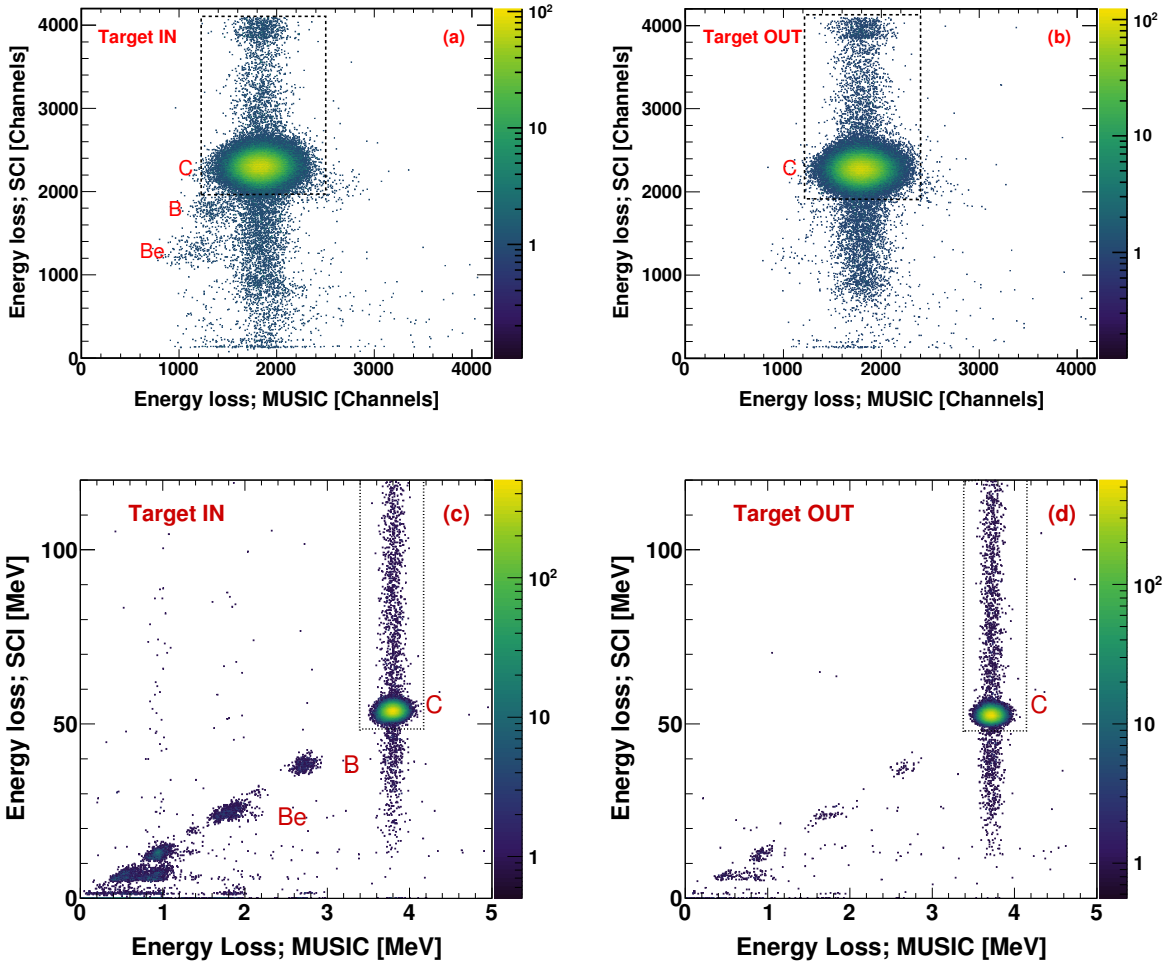

Figure 5. Upper panel: Measured two-dimensional particle identification spectrum showing energy loss in MUSIC versus energy loss in SCI of a ^{10}C beam obtained in the experiment [26], measured with (left) and without (right) a carbon reaction target (1.7 g/cm^2) placed in the beam line at F2. The area enclosed by dotted lines corresponds to unreacted beam particles. Lower panel: Corresponding plots obtained with GEANT4 simulations for the same experimental configurations with the target in (left) and out (right) of the beam line, respectively.

Apart from fragmentation bands, a vertical broadening at constant ΔE_{MUSIC} is observed both with and without the target in experiment as well as in simulations, as shown in Figure 5(a–d). Therefore, it is essential to understand which part should be considered as unreacted to determine σ_{CC}. The identification of events in both the upper and lower tails as carbon ions is confirmed by the MUSIC detector, whose signal scales with Z^2 according to the Bethe–Bloch formalism. The absence of a shift to lower Z bands rules out charge-changing fragmentation processes, indicating that these events correspond to unreacted carbon ions. The observed spread in the scintillator signal can be understood from fluctuations in energy deposition governed by ionization processes, δ-ray production, and variations in effective path length due to low angle scattering and straggling mechanism. Additional contributions arise from non-charge-changing nuclear interactions and detector response effects.

Figure 6(a,b) reflect the correlation between the energy loss measured in plastic scintillator (ΔE) and the measured residual energy deposited in the BaF_2 crystal for the ^{12}C beam with and without three flasks of water target at F4 focal plane of the FRS. The corresponding simulations are shown in Figure 6(c,d). A pronounced locus at high ΔE corresponds to unreacted carbon projectiles (Z=6), as marked as *C* in Figure 6. With similar logic at F2 measurements, particles above this pronounced region (Z=6) are considered as unreacted beam as indicated by dotted lines. Whereas, below the Z=6 region, a diagonal band is observed, originating from the projectile fragmentation into lighter

 doi:10.20944/preprints202604.0374.v1

nuclei (Z < 6). The alignment of the particle in the diagonal band reflects the expected dependence of energy loss on nuclear charge and velocity. Experimentally, the broad distribution of fragment events may be caused by the intrinsic momentum spread of projectile fragmentation products and energy loss-straggling effects. The horizontal elongation in BaF_2 near the carbon locus could be due to intrinsic momentum spread, energy loss-straggling in upstream detector materials, and fragmentation reaction between plastic and BaF_2 crystal. A small variation in the incident energy and particles under large angle can affect the residual energy deposited in BaF_2.

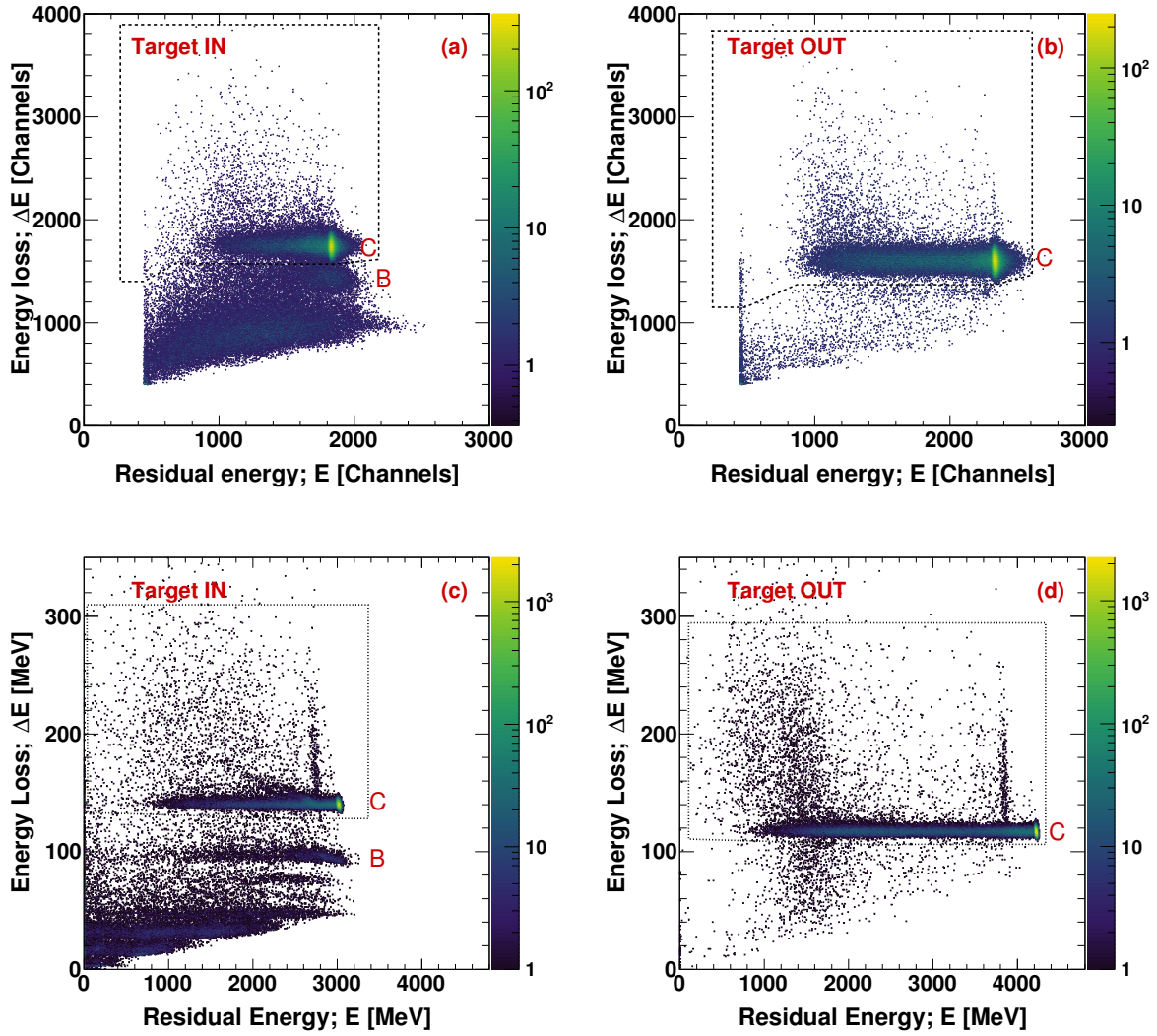

Figure 6. Upper panel: Measured two-dimensional particle identification spectrum showing ΔE versus E for a ^{12}C beam, obtained in the experiment [26], with a 9.6 g/cm^2 water target placed in (left) and out (right) of the beam line. Lower panel: Corresponding comparison with GEANT4 simulations for configurations with the target in (left) and out (right) of the beam line, respectively.

As one can see, e.g., from Figure 6(a–d), the GEANT4 simulations provide a similar level of agreement with respect to the experimental data plots. However, the resolution is even better in GEANT4 simulations.

In the experiment, data without a target were also recorded, accounting for losses due to interactions with non-target materials and for detection efficiencies, which is nicely reproduced by simulations as well. In simulations, a bit observed enhancement (only for a few events in the Z > 6 region) can be attributed to multi-α emission resulting from interactions of beam particles with detector material, such as BaF_2. These processes are described by the ABLA model as sequential evaporation,

 doi:10.20944/preprints202604.0374.v1

where α emission is suppressed relative to neutrons and higher multiplicities are increasingly rare. The associated recoil and negative Q-values broaden and shift the heavy-residue kinematics away from the primary coincidence locus, reducing detection efficiency. Consequently, trigger thresholds and coincidence conditions in the TPC–MUSIC–SCI setup suppress these low yield events in experiment, even though they appear in simulation. In addition, unresolved multi α emission can lead to a reconstructed signal with combined charge and mass comparable to ^{12}C, causing to populate it as carbon like events.

To estimate the systematic uncertainty associated with the determination of the charge-changing cross-section, two independent procedure were implemented in the simulation.

In the first method, the number of unreacted outgoing particles was determined using the response of the downstream scintillator and MUSIC detectors (at F2), including the full beam line geometry and air gap between the target and detector system. Similarly, the counting was done using the E-ΔE detectors at F4 focal plane.

In the second method, the unreacted particles were counted immediately downstream the reaction target, before transport through the beam line.

The resulting cross-sections agree within $\approx 0.1\%$. This deviation is attributed to transport and detector-related effects and is therefore included as a contribution to the systematic uncertainty.

5. Conclusions

The combined experimental analysis and simulations of the energy loss measured in MUSIC-SCI at F2 focal plane and $\Delta E - E$ (plastic-BaF_2) correlations provides a clear and consistent identification of the projectile fragmentation products separated from the unreacted beam ^{12}C. The pronounced locus of the fragment component in the target-in configuration confirm it's origin in nuclear interaction within the target material, while residual broadening effects observed in both target in and out configuration are attributed to the intrinsic beam properties, interactions with air gaps or detector materials, and detector response. A good agreement between measured data and GEANT4 simulations is achieved. Also, independent methods at F2 and F4 focal planes ensure a reliable determination of charge-changing cross-sections and associated systematic uncertainties, demonstrating the robustness of the experimental approach. The associated systematic uncertainty is found to be ≈ 0.1 %.

Funding: This work is supported by European Research Council (ERC) Advanced Grant 883425 (BARB) to Marco Durante.

Data Availability Statement: GEANT4 simulations are associated to this manuscript and data are available on reasonable request.

Acknowledgments: The authors acknowledge the the experiment S533_Purushothaman (SIS18/FRS/S4) within FAIR Phase-0 program for providing raw spectra to benchmark the simulations.

Conflicts of Interest: The authors declare no conflicts of interest.

References

1. Tanihata, I.; Savajols, H.; Kanungo, R. Recent experimental progress in nuclear halo structure studies. *Prog. Part. Nucl. Phys.* **2013**, *68*, 215–313.
2. Otsuka, T.; Gade, A.; Sorlin, O. *et al.* Evolution of shell structure in exotic nuclei. *Rev. Mod. Phys.* **2020**, *92*, 015002.
3. Mizutori, S.; Dobaczewski, J.; Lalazissis, G. A. *et al.* Nuclear skins and halos in the mean-field theory. *Phys. Rev. C* **2000**, *61*, 044326.
4. Sihver, L.; Lantz, M.; Takechi, M. *et al.* A comparison of total reaction cross-section models used in particle and heavy ion transport codes. *Adv. Space Res.* **2012**, *49*, 812–819.
5. Minamisono, T.; Ohtsubo, T.; Minami, I. *et al.* Proton halo of ^{8}B disclosed by its giant quadrupole moment, *Phys. Rev. Lett.* **1992**, *69*, 2058.
6. Tanihata, I.; Kobayashi, T.; Yamakawa, O. *et al.* Measurement of interaction cross sections using isotope beams of Be and B and isospin dependence of the nuclear radii. *Phys. Lett. B* **1988**, *206*, 592–596.

 doi:10.20944/preprints202604.0374.v1

7. Kostyleva, D.; Purushothaman, S.; Dendooven, P. *et al.* Precision of the PET activity range during irradiation with ^{10}C, ^{11}C, and ^{12}C beams. *Phys. Med. Biol.* **2023**, *68*, 015003.
8. Purushothaman, S.; Kostyleva, D.; S.; Dendooven, P. *et al.* Quasi-real-time range monitoring by in-beam PET: A case for ^{15}O. *Sci. Rep.* **2023**, *13*, 18788.
9. Boscolo, D.; Lovatti, G.; Sokol, O. *et al.* Image-guided treatment of mouse tumours with radioactive ion beams. *Nat. Phys.* **2025**, *21*, 1648.
10. Boscolo, D.; Kostyleva, D.; Schuy, C. *et al.* Depth dose measurements in water for ^{11}C and ^{10}C beams with therapy relevant energies. *Nucl. Instrum. Methods Phys. Res. A* **2022**, *1043*, 167464.
11. Geissel, H.; Armbruster, P.; Behr, K.H. *et al.* The GSI projectile fragment separator (FRS): A versatile magnetic system for relativistic heavy ions. *Nucl. Instrum. Methods Phys. Res. B* **1992**, *70*, 286–297.
12. Angert, N.; Schmelzer, Ch. UNILAC, A variable energy linear accelerator for atomic ions of any mass *Kerntechnik* **1969**, *11*, 690–698.
13. Steiner, M.; Blasche, K.; Clerc, H.-G. *et al.* Preliminary measurements of SIS 18 beam parameters, *Nucl. Instrum. Methods Phys. Res. A* **1992**, *312*, 420–432.
14. Bazin, D.; Tarasov, O.; Lewitowicz, M.; *et al.* The program LISE: A simulation of fragment separators. *Nucl. Instrum. Methods Phys. Res. A* **2002**, *482*, 307–327.
15. Janik, R.; Prochazka, A.; Sitar, B. *et al.* Time Projection Chambers with C-pads for heavy ion tracking, *Nucl. Instrum. Methods Phys. Res. A* **2011**, *640*, 54–57.
16. Stolz, A.; Faestermann, T.; Friese, J.; *et al.*, Phys. Rev. C **2002**, *65*, 064603.
17. Pfützner, M. *et al.*, Energy deposition by relativistic heavy ions in thin argon absorbers, *Nucl. Instrum. Methods Phys. Res. B* **1994**, *86*, 213.
18. Agostinelli, S.; Allison, J. *et al. GEANT4—a simulation toolkit*. Nucl. Instrum. Methods Phys. Res. A **2003**, *506*, 250–303.
19. Allison, J.; Amako, K.; Apostolakis, J.; *et al. Recent Developments in GEANT4.* Nucl. Instrum. Meth. A **2016**, *835*, 186–225.
20. Ivantchenko, A. V.; Ivanchenko, V. N.*et al. GEANT4 hadronic physics for space radiation environment.* International Journal of Radiation Biology, **2012**, *88 (1-2)* 171–175.
21. Folger, G.; Ivanchenko, V. N.; *et al. The Binary Cascade.* Eur. Phys. J. A 21, **2004** 407–417.
22. Kaidalov, A. B., *The quark-gluon structure of the pomeron and the rise of inclusive spectra at high energies.* Phys. Lett. B **1982**, *116* 456-463.
23. Gudima, K. K.; S. G. Mashnik; V.D. Toneev *Cascade-exciton model of nuclear reactions.* Nucl. Phys. A, **1983**, *401*, 329-361.
24. Apostolakis, J.; Asai, M.; Bagulya, A. *et al. Progress in GEANT4 Electromagnetic Physics Modelling and Validation.* **2015**, J. Phys.: Conf. Ser. **2015**, *664*, 072021.
25. Hüfner, J.; Schäfer, K.; Schürmann, B. *et al. Abrasion-ablation in reactions between relativistic heavy ions.* Phys. Rev. C **1975**, *12*, 1888–1898.
26. Purushothaman, S. *et al. Measurements of nuclear and atomic interactions needed for ion-beam therapy with positron emitters of carbon. GSI Proposal S533, GSI Darmstadt, Germany, 2021.*
27. Cervantes, Y.; Lambert-Girard, S. *et al. A systematic characterization of plastic scintillation dosimeters response in magnetic fields: II. Monte Carlo simulations.* Phys. Med. Biol. **2025**, *70*, 105004.